ARTICLE

Pt/TiO_2 Nanosheets Array Dominated by $\{001\}$ Facets with Enhanced Photocatalytic Activity

Feng Li[a], Zheng-ping Fu[a*], Ya-lin Lu[a,b*]

a. CAS Key laboratory of Materials for Energy Conversion, Department of Materials Science and Engineering, University of Science and Technology of China, Hefei 230026, China
b. National Laboratory for Physical Sciences at the Microscale, University of Science and Technology of China, Hefei 230026, China

(Dated: Received on May 11, 2014; Accepted on June 6, 2014)

{001} facets dominated single crystalline anatase TiO_2 nanosheet array (TNSA) was synthesized through an optimized organic solvothermal route on fluorine-doped tin oxide substrate. The field emission scanning electron microscopy images and X-ray diffraction patterns revealed that the {001} synthesized facets dominated TNSA exhibited much higher orientation than that synthesized by hydrothermal route. The TNSAs were loaded with Pt nanoparticles in uniformly size by using a photodecomposition method, which were further confirmed by high resolution transmission electron microscopy (HRTEM). The HRTEM images also revealed that Pt nanoparticles preferred to deposit on {001} facets. With loading of Pt nanoparticles, the optical absorbance was significantly enhanced, while the photoluminescence (PL) was inhibited. The photocatalytic activity of TNSA was significantly improved by Pt loading and reached the maximum with optimal amount of Pt loading. The optimal amount of Pt on {001} facets is far less than that on TiO_2 nanoparticles, which may be attributed to the specific atom structure of reactive {001} facets.

Key words: Organic solvothermal route, Photodecomposition, TiO_2, Nanosheet array, {001} facet

I. INTRODUCTION

Owing to their potential applications in photocatalysis, hydrogen production, dye-sensitized solar cells, single crystalline TiO_2 nanostructure with special morphology and orientation have attracted much more attention in recent years. In particular, reactive facets dominated TiO_2 are more preferred. However, reactive facets are usually unavailable, which will disappear in the crystalline growth process [1−3]. Recently, Yang and coworkers successfully synthesized {001} facets dominated anatase TiO_2 nanosheets using hydrofluoric acid as capping agent [4]. Compared with P25, {001} facets dominated TiO_2 nanosheets exhibited 5 times higher photocatalytic activity [5]. Since then, great efforts have been devoted to the synthesis of {001} facets dominated TiO_2 [6−8].

The photocatalytic activity of TiO_2 is still low, mainly because of the recombination of photogenerated electrons and holes. Many strategies have been developed to enhance the photocatalytic activity of TiO_2 [9]. Among them, noble metal loading is one of the best known methods to enhance the separation of photogenerated electrons and holes [10−13]. Most of previous studies focused on noble metals deposition on conventional TiO_2 films or P25 powder [10, 14−16], while few works has been done on the deposition of noble metals on TiO_2 dominated by reactive facets, especially TiO_2 nanosheet array (TNSA) dominated by {001} facets. On the other hand, compared with thermal decomposition method and alcohol reduction method, photodeposition method can selectively deposit noble metals on specific facets [17], which may lead to distinct and enhanced photocatalytic performance.

Herein, we reported an optimized organic solvothermal method to synthesis {001} facets dominated TNSA on fluorine-doped tin oxide substrate (FTO). The obtained TNSA were further loaded with different amount of Pt through the photodeposition method [18]. It was demonstrated that {001} facets were more preferred by Pt nanoparticles in the photodeposition method. The Pt loading also had an optimal amount, with which the Pt-TNSA show much higher photocatalytic activity in the photodegradation of methylene blue (MB). The optimal amount of Pt loading is very tiny, which may can be attributed to the specific atom structure of reactive {001} facets.

*Authors to whom correspondence should be addressed. E-mail: fuzp@ustc.edu.cn, yllu@ustc.edu.cn

II. EXPERIMENTS

In a typical synthesis, the FTO coated glass was ultrasonically cleaned sequentially in acetone, ethanol, distilled water for 20 min each, subsequently immersed in a 1 mol/L NaOH aqueous solution for 24 h, then rinsed with distilled water, and finally dried in the air. A TiO_2 seed layer was prepared on the as-cleaned FTO coated glass by spin coating method. Separately, 1.5 mL of titanium butoxide was added drop-wise to 20 mL of toluene. The mixture was stirred at ambient conditions for 5 min before the addition of 0.6 mL of hydrofluoric acid. After stirring for another 5 min, the mixture was transferred to a dried 50 mL Teflon-lined autoclave within three pieces of FTO coated glass substrates placed vertically, and kept at 180 °C for 24 h. After synthesis, the TNSA samples were taken out, washed with ethanol and distilled water, then dried in air.

The obtained TNSAs were immersed in the chloroplatinic acid solutions with a series of concentration (0.2, 0.5, 1.0, 5.0 mmol/L) under 60 °C for 3 h in the dark. Subsequently, the TNSAs were further irradiated by a 20 W UV lamp with dominant wavelength of 254 nm, the distance between lamp and TNSA was 10 cm. After 10 min irradiation, the TNSAs were taken out and washed with distilled water for several times, and named as PTNSA-0.2, PTNSA-0.5, PTNSA-1, and PTNSA-5.

The photocatalytic activities of the as-synthesized samples were tested on the degradation of methylene blue (MB) under UV light irradiation. A 20 W UV lamp with dominant wavelength of 254 nm was used as UV resource. The samples with the same geometric area (1.5 cm×1.0 cm) were laid in a culture dish containing 50 mL MB solutions with concentrations of 2 mg/L. Prior to irradiation, MB solutions were stirred in the dark for 30 min to achieve an adsorption-desorption equilibrium. MB solutions were sampled for determining concentration after 0, 30, 60, 90, and 120 min of irradiation respectively. The concentrations of MB solution samples were further monitored by measuring the maximum absorbance at a wavelength of 664 nm via UV-Vis spectrophotometer.

XRD patterns were obtained by using a TTR-III X-ray diffractometer with Cu Kα radiation (λ=1.5418 Å). The morphologies of TNSAs were examined by field emission scanning electron microscopy (FESEM, JSM-6700F) and high resolution transmission electron microscopy (HRTEM, JEOL-2010). UV-Vis absorption spectra were measured on a UV-Vis spectrophotometer (Unico UV-2400AH). The photoluminescence (PL) spectra of the samples were obtained using a fluorescent spectrophotometer (F-4600) with a 200 W Xe lamp as the excitation source at an excitation wavelength of 254 nm.

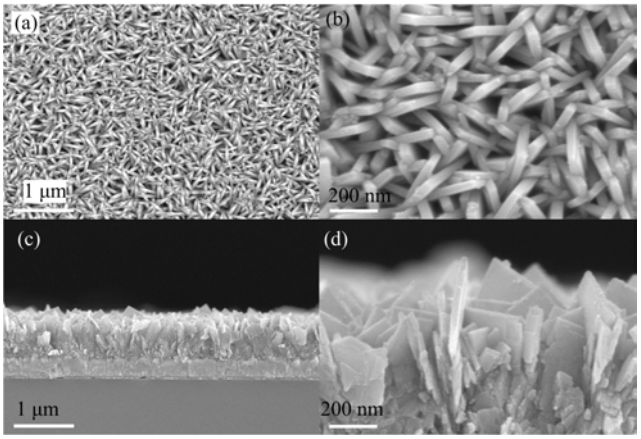

FIG. 1 Low and high magnification FESEM images of TNSA from top view (a, b) and side view (c, d).

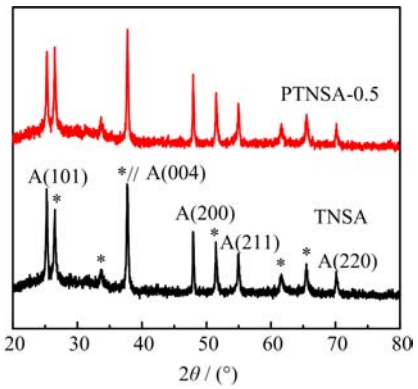

FIG. 2 XRD patterns of TNSA and PTNSA-0.5. Diffraction peaks marked with stars belong to FTO substrate.

III. RESULTS AND DISCUSSION

The morphology of TNSA is shown in Fig.1 from top and side views. The as-prepared TNSA is assembled by nanosheets, which are nearly perpendicular to the substrate. Each nanosheet has a side length of 400−450 nm and a laminar thickness of 20−25 nm. The nanosheets support each other, keeping the TNSA array from aggregating and collapsing. Compared with TNSA prepared by hydrothermal route using water as the solvent [19], TNSA prepared by toluene solvothermal route seems to be more uniformly and vertically stood, which may be attributed to the smaller surface tension of toluene.

As shown in Fig.2, the crystal structure of TNSA was studied by X-ray diffraction (XRD). All of the indicated diffraction peaks of TNSA can be attributed to the anatase TiO_2 (JCPDF, No. 89-4921, a=b=0.3777 nm, c=0.9501 nm). The diffraction peaks which should present in the XRD pattern of polycrystal, such as (103), (112), (105), (204), and (215), are absent, indicating the highly orientation of the nanosheets. Meanwhile, the intensity ratio of (101) to (200) diffraction

DOI:10.1063/1674-0068/27/05/530-534

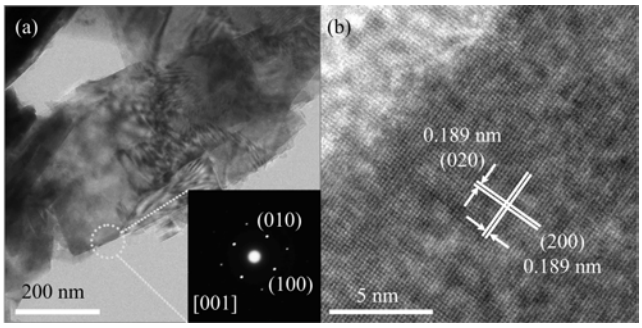

FIG. 3 (a) Low magnification TEM images of nanosheets in TNSA and corresponding SAED pattern, (b) high magnification TEM images of TiO_2 nanosheet in TNSA.

peaks in our work was less than 1.5:1, while it was almost 4:1 in Feng's work [19], and (105), (204), (116), (215) diffraction peaks also appeared in their XRD pattern. This result revealed that TNSA in our work exhibited much higher orientation, which can be attributed to the improved organic solvothermal route. TNSA with Pt loading, PTNSA-0.5, was also investigated by XRD. However, the loading amount of Pt was under the detection limit of XRD technique, while diffraction peaks of Pt were obvious in Chen and Zhang's works [18, 20−22].

Crystal characteristic of the TNSA was investigated. The morphology of nanosheets is shown in Fig.3(a), the nanosheets stacked together during the TEM sample preparation process. The side length of the nanosheet is about 400 nm, agrees well with the SEM information. The corresponding selected area electron diffraction (SAED) pattern, can be indexed as ⟨001⟩ zone diffraction, revealing that the nanosheet is single crystal. Lattice spacing of fringes in Fig.3(b) are 0.189 nm, corresponding to the {200} and {020} facets of anatase TiO_2. The fringes appearing in pairs show an included angle of 90°, identifying {001} facet as the surface of nanosheet. Based on the XRD and TEM information, we conclude that the nanosheet are {001} facets dominated single crystalline anatase TiO_2 nanosheet. The appearance of {001} facets can be attributed to the F-adsorption during the crystal growth process, which can minimize the surface energy [4].

To further investigate the microstructures of the Pt loaded nanosheets, the TEM technique was adopted. Figure 4(a) shows the morphology of Pt loaded nanosheets, the nanosheets stacked together during the TEM sample preparation process. Lattice spacing of fringes in Fig.4(b) are 0.3777 nm, corresponding to the {100} facets of anatase TiO_2. The fringes appearing in pairs show an included angle of 90°, identifying {001} facet as the surface of nanosheet. Corresponding FFT pattern of Fig.4(b) is shown in Fig.4(c), further confirming the ⟨001⟩ axis as the diffraction axis. Nanoparticles marked with white circles in Fig.4(b) are photodeposited Pt, magnified in Fig.4(d). As shown, lattice spacing of the fringes in Fig.4(d) is 0.222 nm, which

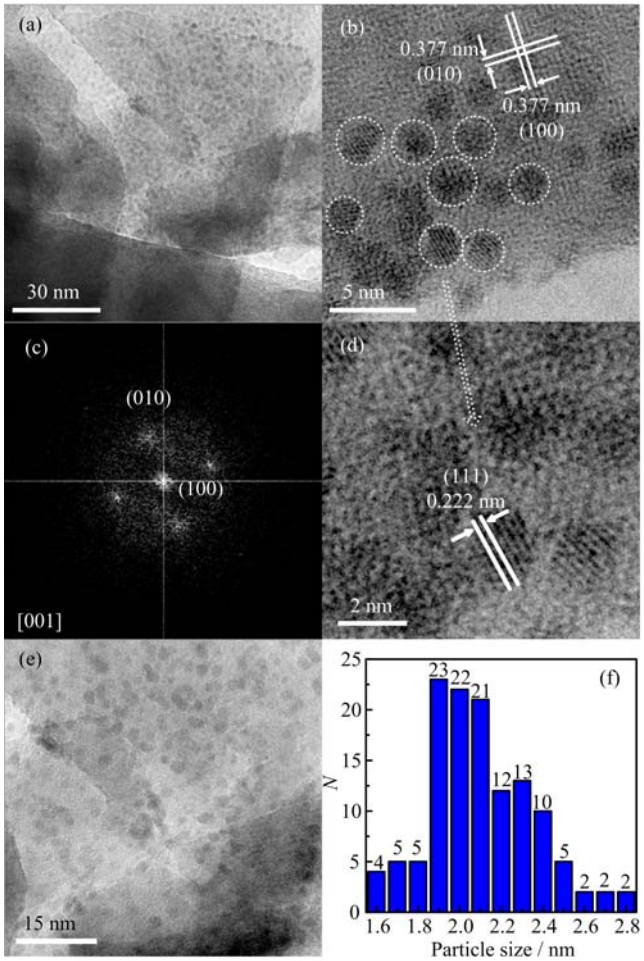

FIG. 4 (a) Low magnification TEM images of nanosheets in PTNSA-0.5. (b) High magnification TEM image of TiO_2 nanosheet in PTNSA-0.5. (c) FFT pattern of (b). (d) High magnification TEM images of Pt nanoparticles. (e) Low magnification TEM images of Pt nanoparticles. (f) Size distribution of Pt nanoparticles in (e).

belongs to the {111} facets of Pt. Compared with the edge, {001} facets surface seems to be more preferred by Pt nanoparticles. Figure 4(e) shows low magnification TEM images of Pt nanoparticles, and corresponding size distribution is shown in Fig.4(f). Benefitting from photodecomposition process, the sizes of Pt nanoparticles are uniform with an average size of about 2 nm.

The UV-Vis absorption spectra of the TNSA and PTNSA-0.5 are shown in Fig.5. In UV light region, the absorbance of TNSA and PTNSA-0.5 appears to be similar to each other. Compared with TNSA, the absorbance of TNSA loaded by Pt nanoparticles is enhanced in the visible light region, which can be attributed to resonance of collective excitations of conduction electrons of noble metal nanoparticles with the incident photo frequency, so called the localized surface plasmon resonance (LSPR) [23]. Especially, in PTNSA-0.5, a weak plasma absorption peak appears

DOI:10.1063/1674-0068/27/05/530-534

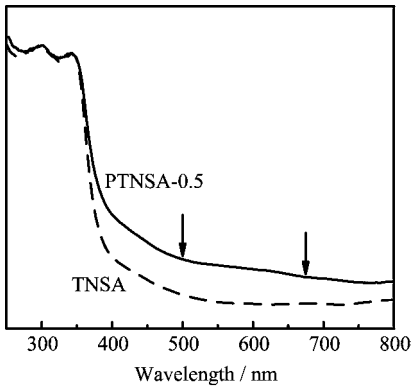

FIG. 5 UV-Vis absorption spectra of PTNSA-0.5 and TNSA.

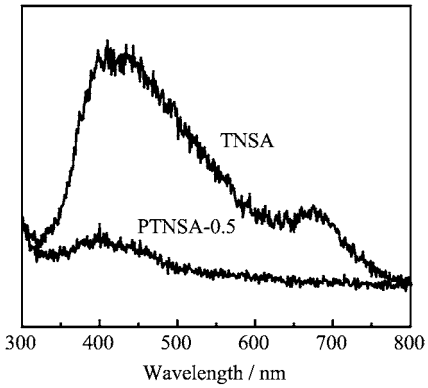

FIG. 6 Photoluminescence spectra of PTNSA-0.5 and TNSA. The excitation wavelength is 254 nm.

at 500−675 nm (indicated with arrows in Fig.5), which can be attributed to the tiny amount of Pt loading, may lead to visible light photocatalytic activity.

Photoluminescence (PL) spectra of TNSA and PTNSA-0.5 were measured by a fluorescence spectrophotometer (Hitachi F-4600) with an excitation wavelength of 254 nm. As shown in Fig.6, TNSA without Pt loading shows a strong and broad-band emission from 350−750 nm, indicating serious recombination of electrons and holes. Generally, a lower PL intensity indicates a lower recombination rate of electrons and holes, or in other words, improved separation of the photogenerated carriers. Therefore, the PL results show that Pt loading remarkably reduced the recombination of electrons and holes in TNSA. On the other hand, the loading of Pt exists an optimal amount, overloaded Pt serves as new recombination center, and increases the recombination of electrons and holes [24].

The photocatalytic activities of samples were investigated by photo-degradation of MB under UV light irradiation for a series of time. As shown in Fig.7, after 120 min irradiation, PTNSA-0.5 exhibits the highest degradation rate (30%), suggesting that PTNSA-0.5 has the optimal amount of Pt loading, while others exhibit lower degradation rate. Compared with conventional Pt loading [20−22], the optimal amount of Pt loading on {001} facets to reach the best photocatalytic performance is far less and even under the detection limit of XRD, which may be attributed to the specific atom structure of the {001} facets. Compared to {101} facets which dominate in conventional TiO_2, {001} facets possess much more five coordinated Ti atoms and are much more reactive, and Pt loading will reduce these corresponding reactive sites [25]. As a shifting of the competition, far less amount of Pt loading is need to achieve the optimal photocatalytic performance.

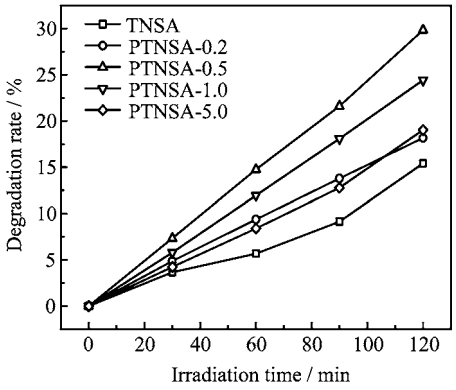

FIG. 7 Degradation of MB under UV light irradiation with TNSA, PTNSA-0.2, PTNSA-0.5, PTNSA-1, and PTNSA-5 for a series of irradiation time.

IV. CONCLUSION

We have developed an optimized organic solvothermal route to synthesize highly oriented TNSA, which is dominated by reactive {001} facets. Serial amounts of Pt were loaded on the TNSA through photodecomposition method, and Pt nanoparticles preferred to deposit on {001} facets. Compared with conventional TiO_2, less amount of Pt loading is need to optimize the photocatalytic performance on nanosheets dominated with {001} facets, which may be attributed to the specific atom structure of reactive {001} facets. The strategy to study the characteristic of specific facets provides an alternative route to facets research and can be extended to other materials, leading to well understanding of their specific facets.

V. ACKNOWLEDGMENTS

This work is supported by the National Basic Research Program of China (No.2012CB9222000).

[1] F. Han, V. S. R. Kambala, M. Srinivasan, D. Rajarathnam, and R. Naidu, Appl. Catal. A **359**, 25 (2009).

DOI:10.1063/1674-0068/27/05/530-534

[2] A. Fujishima and K. Honda, Nature **238**, 37 (1972).
[3] G. K. Mor, O. K. Varghese, M. Paulose, K. Shankar, and C. A. Grimes, Sol. Energ. Mat. Sol. C **90**, 2011 (2006).
[4] H. G. Yang, C. H. Sun, S. Z. Qiao, J. Zou, G. Liu, S. C. Smith, H. M. Cheng, and G. Q. Lu, Nature **453**, 638 (2008).
[5] G. Liu, C. H. Sun, H. G. Yang, S. C. Smith, L. Z. Wang, G. Q. Lu, and H. M. Cheng, Chem. Commun. **46**, 755 (2010).
[6] S. J. Ding, J. S. Chen, Z. Y. Wang, Y. L. Cheah, S. Madhavi, X. A. Hu, and X. W. Lou, J. Mater. Chem. **21**, 1677 (2011).
[7] W. Q. Fang, J. Z. Zhou, J. Liu, Z. G. Chen, C. Yang, C. H. Sun, G. R. Qian, J. Zou, S. Z. Qiao, and H. G. Yang, Chem. Eur. J. **17**, 1423 (2011).
[8] W. G. Yang, J. M. Li, Y. L. Wang, F. Zhu, W. M. Shi, F. R. Wan, and D. S. Xu, Chem. Commun. **47**, 1809 (2011).
[9] H. J. Zhang, G. H. Chen, and D. W. Bahnemann, J. Mater. Chem. **19**, 5089 (2009).
[10] I. Tanahashi, F. Yamazaki, and K. Hamada, Chem. Lett. **35**, 454 (2006).
[11] V. Subramanian, E. Wolf, and P. V. Kamat, J. Phys. Chem. B **105**, 11439 (2001).
[12] J. B. Lowekamp, G. S. Rohrer, P. A. M. Hotsenpiller, J. D. Bolt, and W. E. Farneth, J. Phys. Chem. B **102**, 7323 (1998).
[13] P. Claus and H. Hofmeister, J. Phys. Chem. B **103**, 2766 (1999).
[14] L. B. Yang, X. Jiang, X. D. Ruan, J. X. Yang, B. Zhao, W. Q. Xu, and J. R. Lombardi, J. Phys. Chem. C **113**, 16226 (2009).
[15] S. L. Zou and G. C. Schatz, J. Chem. Phys. **121**, 12606 (2004).
[16] M. Wu, B. F. Yang, Y. Lv, Z. P. Fu, J. A. Xu, T. Guo, and Y. X. Zhao, Appl. Surf. Sci. **256**, 7125 (2010).
[17] R. G. Li, F. X. Zhang, D. E. Wang, J. X. Yang, M. R. Li, J. Zhu, X. Zhou, H. X. Han, and C. Li, Nature Commun. **4**, 1432 (2013).
[18] J. G. Yu, L. F. Qi, and M. Jaroniec, J. Phys. Chem. C **114**, 13118, (2010).
[19] S. L. Feng, J. Y. Yang, H. Zhu, M. Liu, J. S. Zhang, J. Wu, and J. Y. Wan, J. Am. Ceram. Soc. **94**, 310 (2011).
[20] Y. X. Zhao, B. F. Yang, J. Xu, Z. P. Fu, M. Wu, and F. Li, Thin Solid Films **520**, 3515 (2012).
[21] W. Mu, J. M. Herrmann, and P. Pichat, Catal. Lett. **3**, 73 (1989).
[22] P. Chen and X. G. Zhang, Clean-Soil Air Water **36**, 507 (2008).
[23] J. L. Zhang, Z. F. Yuan, B. S. Xu, and P. F. Fu, Adv. Appl. Ceram. **109**, 362 (2010).
[24] X. C. Wang, J. C. Yu, H. Y. Yip, L. Wu, P. K. Wong, and S. Y. Lai, Chem. Eur. J. **11**, 2997 (2005).
[25] H. Xu, P. Reunchan, S. X. Ouyang, H. Tong, N. Umezawa, T. Kako, and J. H. Ye, Chem. Mater. **25**, 405 (2013).

DOI:10.1063/1674-0068/27/05/530-534